Proceeding Paper

Eugenol Ester Derivatives: Synthesis, Insecticidal Activity and Computational Studies †

José R. A. Coelho [1], Tatiana F. Vieira [2,3], Renato B. Pereira [4], David M. Pereira [4], Elisabete M. S. Castanheira [5], A. Gil Fortes [1], Sérgio F. Sousa [2,3], Maria José G. Fernandes [1] and M. Sameiro T. Gonçalves [1,*]

[1] Centre of Chemistry (CQ/UM), University of Minho, Campus of Gualtar, 4710-057 Braga, Portugal; a85799@alunos.uminho.pt (J.R.A.C.); gilf@quimica.uminho.pt (A.G.F.); mjfernandes@quimica.uminho.pt (M.J.G.F.)

[2] Associate Laboratory i4HB—Institute for Health and Bioeconomy, Faculty of Medicine, University of Porto, 4200-319 Porto, Portugal; tatianafvieira@gmail.com (T.F.V.); sergiofsousa@med.up.pt (S.F.S.)

[3] UCIBIO—Applied Molecular Biosciences Unit, BioSIM—Department of Biomedicine, Faculty of Medicine, University of Porto, Alameda Prof. Hernâni Monteiro, 4200-319 Porto, Portugal

[4] REQUIMTE/LAQV, Laboratory of Pharmacognosy, Department of Chemistry, Faculty of Pharmacy, University of Porto, R. Jorge Viterbo Ferreira, 228, 4050-313 Porto, Portugal; ren.pereira@gmail.com (R.B.P.); dpereira@ff.up.pt (D.M.P.)

[5] Centre of Physics of Minho and Porto Universities (CF-UM-UP), University of Minho, Campus of Gualtar, 4710-057 Braga, Portugal; ecoutinho@fisica.uminho.pt

* Correspondence: msameiro@quimica.uminho.pt

† Presented at the 25th International Electronic Conference on Synthetic Organic Chemistry, 15–30 November 2021; Available online: https://ecsoc-25.sciforum.net/).

Abstract: Specific structural modifications in eugenol molecule can simultaneously improve the biological activity and reduce side effects of the respective analogues. The esterification of eugenol by two different experimental procedures, and subsequently conversion of one of the esters into the corresponding oxirane was carried out. All derivatives obtained were then evaluated for their effect on the viability of *Sf9* (*Spodoptera frugiperda*), cells. In addition, a structured-based inverted virtual screening protocol was employed to identify the potential proteins associated to the observed insecticidal activity. The encouraging results obtained allowed to establish a preliminary structure-activity relationship.

Keywords: eugenol; eugenol derivatives; *Spodoptera frugiperda*; insecticidal activity; computational studies

1. Introduction

Due to the exponential increase in world population, it is necessary to ensure agricultural production that meets the actual food requirements. The improvement in the productivity of agricultural crops implies an incessant need to prevent, control and destroy the pests that affect them, achieved through the extensive use of synthetic pesticides. Although synthetic pesticides represent a plausible approach, they present a serious threat because their uncontrolled use causes negative impacts on the environment (pollution and loss of biodiversity) and on human health [1,2].

Natural products are good alternatives, due to the structural diversity and associated biological activity, so as they are a rich source of inspiration in the design and optimization of active principles in the development of formulations, highlighting the crucial role of plant extracts [3,4]. In this category, essential oils fit perfectly, exhibiting a broad-spectrum of actions, including antibacterial, antifungal, insecticidal and antioxidant activities, as for example eugenol [5,6].

Considering these facts, and as a continuation of our recent interests in alternative pesticides, eugenol derivatives were obtained through esterification and epoxidation reactions and evaluated for their effect on the viability of *Sf9* cells. A structure-based inverted virtual screening protocol was employed to identify the potential proteins associated to the observed insecticidal activity.

2. Results and Discussion

2.1. Synthesis of Eugenol Derivatives 2a-c and 3

4-Allyl-2-methoxyphenol, eugenol **1**, was the lead compound used in the synthesis of three *O*-esterified derivatives **2a-c**, which compound **2b** was then converted in the respective oxirane **3** as shown in Scheme 1. The esterification of 4-allyl-2-methoxyphenol **1** in basic conditions with *m*-nitrobenzoyl chloride and *p*-nitrobenzoyl chloride gave 4-allyl-2-methoxyphenyl 3-nitrobenzoate **2a** and 4-allyl-2-methoxyphenyl 4-nitrobenzoate **2b**, as solids in 72 and 49% yields, respectively. In addition, compound 1 was also esterified with *p*-anisic acid, by using dicyclohexylcarbodiimide (DCC) and 4-(dimethylamino)pyridine (DMAP), in dichloromethane, at room temperature, resulting the 4-allyl-2-methoxyphenyl 4-methoxybenzoate **2c** as a solid material in 69% yield.

Epoxidation of the double bond of compound **2b** with *m*-perchloroperbenzoic acid in dichloromethane at room temperature, resulted in 2-methoxy-4-(oxiran-2-ylmethyl)phenyl 4-nitrobenzoate **3**, isolated with 31% yield. Compounds **2a-c** and **3** were fully characterized by the usual analytical techniques. The ^{1}H NMR showed the signals of aromatic protons derived from the eugenol unity (δ 6.81–7.12 ppm), in addition to the protons of the nitro- or methoxyphenyl rings, highlighting H-2 and H-5 displayed as triplets or multiplets (δ 8.34–9.06 ppm, H-2; δ 6.84–7.75 ppm, H-5) for compounds **2a** and **2b**, respectively, and as dublets (δ 8.18 ppm, H-2; δ 6.99 ppm, H-5) for compound **2c**. The alkene protons are showed as multiplets (δ 5.10–6.03 ppm) in compounds **2a-c**, and are absent in compound **3**, giving way to the oxirane ring protons, showed as quartet and multiplets (δ 2.58–3.23 ppm). The ^{13}C NMR also confirm the presence of the ester bond (δ 162.96–164.62 ppm) in all compounds, as well as the oxirane ring in compound **3** (δ 46.79–52.28 ppm).
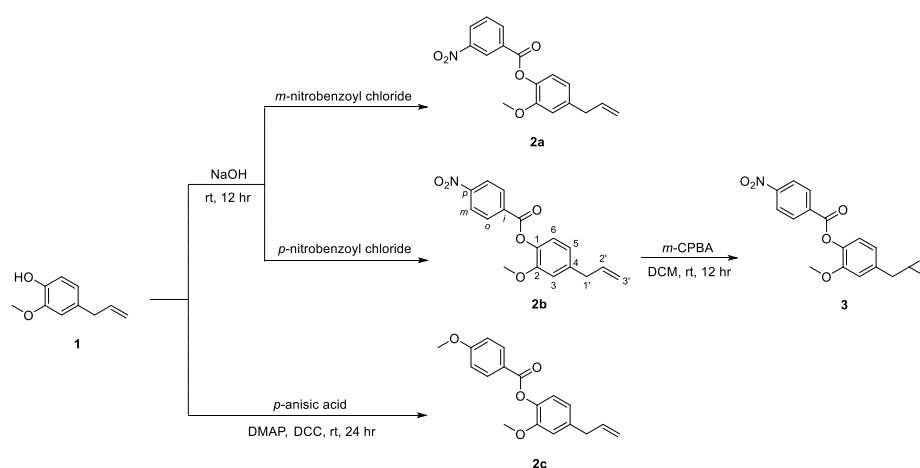
Scheme 1. Synthesis of eugenol derivatives **2a-c** and **3**.

2.2. Biological Activity of Compounds 2a-c and 3 in Sf9 Insect Cells

Aiming the evaluation of the insecticidal activity of the synthesized eugenol derivatives **2a-c** and **3**, studies were carried out in *Spodoptera frugiperda* (*Sf9*) cells, a common pest widely used on the screening of insecticides. For benchmarking purposes, the insecticide chlorpyrifos (CHPY) was used at the same concentration (100 µg/mL). As can be seen in Figure 1, it is clear that the esterification of eugenol with a nitrobenzene group pontentiate eugenol toxicity, derivatives under study displaying equivalent (compound **2a**) or even

higher (compound **2b** and **3**) toxicity than the commercial insecticide, CHPY (Figure 1). Noteworthy, when the nitro group linked to the benzene ring (compound **2b**) is replaced by a methoxy group (compound **2c**), the cytotoxicity is completely lost. On the other hand, oxirane formation (compound **3**) lead to a slight increase in toxicity (Figure 1).
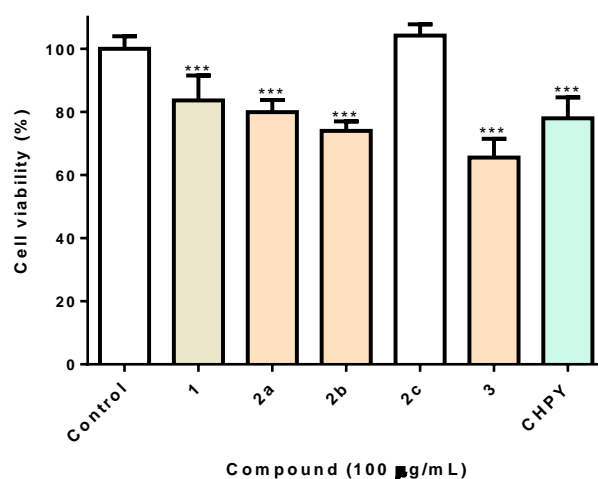

Figure 1. Viability of *Sf9* insect cells exposed to the molecules under study **2a-c** and **3** (100 µg/mL), or medium (control) or the reference insecticide chlorpyrifos (CHPY). *** $p < 0.001$.

2.3. Inverted Virtual Screening Results

Table 2 presents the average scores obtained for the four eugenol derivatives for each potential target calculated with each SFs. Regarding the difference in the values, it must be stated that different SFs are based on different scales and metrics. The score for all the GOLD scoring functions is dimensionless with a higher score yielding a better binding affinity. Vina, on the other hand, uses a metric that is a more precise approximation of binding free energy, meaning that a more negative value is equivalent to better affinity.

Table 2. Average eugenol derivate scores obtained for all PDB structures with the six different scoring functions.

Target	PDB	PLP	ASP	Chem-Score	GoldScore	Vina	Overall Ranking
Acetylcholinesterase	1QON	76.71	56.76	38.14	61.43	−9.63	
	4EY6	76.16	51.57	38.88	57.98	−9.00	2
	1DX4	76.32	50.62	35.14	63.56	−9.33	
alpha-Esterase-7 (αE7)	5TYJ	62.07	36.72	28.51	55.37	−7.33	7
	5TYP	63.49	40.84	31.42	55.85	−7.15	
beta-*N*-Acetyl-D-hexosaminidase OfHex1	3NSN	75.83	54.25	32.29	58.32	−7.63	4
	3OZP	70.09	50.77	30.95	61.58	−8.55	
Chitinase	3WL1	74.64	48.90	33.49	61.49	−8.28	3
	3WQV	74.20	47.85	33.40	64.67	−8.55	
Ecdysone receptor	1R20	71.10	32.79	32.22	56.77	−8.03	5
	1R1K	69.64	35.64	34.15	60.76	−8.78	
N-Acetylglucosamine-1-phosphate uridyltransferase (GlmU)	2V0K	54.77	25.78	23.49	53.69	−7.20	12
	2VD4	47.41	26.34	22.46	42.93	−5.98	
Octopamine receptor	4N7C	47.39	33.06	27.26	47.53	−5.90	13
Odorant Binding Protein	5V13	84.80	52.54	40.54	65.30	−9.13	1
	2GTE	65.44	37.13	36.20	61.29	−8.15	

	3N7H	80.79	44.86	30.52	69.46	−7.45	
	3K1E	85.76	46.38	35.88	71.78	−7.20	
Peptide deformylase	5CY8	69.29	32.36	24.45	61.43	−7.93	8
p-Hydroxyphenylpyruvate di-oxygenase	6ISD	63.44	38.44	28.09	52.91	−8.10	9
Polyphenol oxidase	3HSS	54.54	29.27	24.58	64.34	−6.75	10
Sterol carrier protein-2 (HaSCP-2)	4UEI	65.99	34.95	31.54	52.99	−8.25	6
Voltage-gated sodium channel	6A95	61.46	25.01	23.35	58.99	−7.33	11

Generally, the results show good consistency between SFs, with odorant binding proteins, acetylcholinesterases, chitinases and beta-*N*-acetyl-D-hexosaminidase yielding better scores. On the other hand, targets such as octopamine receptor, *N*-acetylglucosamine-1-phosphate uridyltransferase (GlmU) and voltage-gated sodium channels, consistently present lower scores for across all the SFs.

From each set of targets, the structure with the best score was selected and ranked from the best target to worst, according to the predictions of the different SFs. The overall ranking is listed in Table 2. Globally, considering the results obtained with the several SFs, odorant binding proteins are the most likely target with the highest affinity towards eugenol derivatives, followed closely by acetylcholinesterases. The discrepancy in some of the values of the different SFs, can be explained by the own nature of each SF, as they consider different aspects of protein-ligand binding.

The hypothesis formed is that eugenol and eugenol derivatives can be used as repellents because they can bind to odorant binding proteins or used as pesticides, inhibiting insect acetylcholinesterase.

Interestingly, in the PDB database there is a structure of an odorant binding protein bound to eugenol Apis mellifera (PDB: 3S0E) [7]. This might be an important indicator of the increased affinity of eugenol derivatives against OBPs.

2.4. Molecular Dynamics Simulations and Free Energy Calculations Results

In order to validate the inverted VS predictions, molecular dynamics simulations were then performed for the eugenol derivatives complexes formed with the two groups of targets predicted at the inverted VS stage: odorant binding proteins and acetylcholinesterases. The structure with the best score from each group was selected (3K1E for OBP and 1QON for acetylcholinesterases—AChE). The results are detailed in Table 3.

Table 3. Average RMSD values (Å), average ligand RMSD (Å), average SASA (Å2), percentage of potential ligand SASA buried and an average number of hydrogen bonds for the ligands for the last 70 ns of the simulation of the OBP and AChE-ligand complexes.

		Average RMSD of the Complex (Å)	Average RMSD of the Ligand (Å)	Average SASA (Å²)	Percentage of Potential Ligand SASA Buried (%)	Average Number of Hbonds	ΔGbind (kcal/mol)	Main Contributors (kcal/mol)
OBP	2a	2.0 ± 0.2	0.8 ± 0.2	69.2 ± 15.2	87	0.01 ± 0.05	−37.7 ± 0.1	Trp105 (−3.2 ± 0.6); Leu67 (−2.2 ± 0.4); Met82 (−1.5 ± 0.4)
	2b	2.2 ± 0.2	0.8 ± 0.2	70.2 ± 12.9	87	0.01 ± 0.1	−38.6 ± 0.1	Trp105 (−3.1 ± 0.5); Leu67 (−1.7 ± 0.5); Ile78 (−1.7 ± 0.6)

	2c	2.2 ± 0.2	0.6 ± 0.1	59.6 ± 13.5	89	0.01 ± 0.1	−37.2 ± 0.1	Trp105 (−2.6 ± 0.5); Leu67 (−1.9 ± 0.4); Ile78 (−1.6 ± 0.6)
	3	2.0 ± 0.1	0.8 ± 0.3	59.6 ± 13.5	89	0.01 ± 0.1	−39.7 ± 0.1	Trp105 (−3.2 ± 0.5); Leu67 (−1.9 ± 0.4); Ile78 (−1.8 ± 0.5)
AChE	**2a**	2.9 ± 0.2	0.9 ± 0.2	39.1 ± 9.9	93	0.01 ± 0.3	−25.4 ± 0.1	Tyr69 (−1.4 ±0.6); Gly148 (−1.2 ± 0.5); Tyr322 (−1.0 ± 0.5)
	2b	2.9 ± 0.4	1.3 ± 0.2	68.2 ± 21.2	88	0.3 ± 0.5	−29.2 ± 0.2	Tyr372 (−3.0 ± 0.8); Trp81 (−2.0 ± 0.9); Tyr69 (−1.6 ± 0.5)
	2c	2.9 ± 0.4	0.9 ± 0.2	51.1 ± 12.8	90	0.7 ± 0.9	−27.3 ± 0.2	Trp81 (−2.3 ± 0.5); Tyr69 (−1.7 ± 1.0); Tyr368 (−1.6 ± 1.1)
	3	3.6 ± 0.3	1.0 ± 0.3	39.3 ± 13.1	93	0.1 ± 0.3	−31.7 ± 0.2	Trp81 (−2.7 ± 0.5): Gly148 (−1.2 ± 0.5); Tyr372 (−1.2 ± 0.4)

The OBP-eugenol derivatives complexes are very stable throughout the simulation and presented an average protein RMSD around 2 Å. The prediction from the inverted VS were confirmed as the ligand RMSD is very low. For AChE-eugenol derivatives, however, the average RMSD is higher, indicating that the system shifted to a more stable conformation in the beginning of the simulation. Also, the inverted VS predictions were validated for this target, as the average ligand RMSD values are bellow or equal to 1 Å.

The average SASA and percentage of potential ligand SASA buried indicate the ligand exposure to solvent, so, and increased SASA and a lower percentage of ligand buried, the more solvent exposure. Compounds **2c** and **3** are the ones that are less exposed to the solvent and more buried in the binding pocket of OBP. Regarding AChE, the compounds that are less exposed and more buried in the active site are **2a** and **3**.

Generally, the Gibbs free energy of association was better for OBP-eugenol derivatives than for AChE-eugenol derivatives. Compounds **2a** and **3** are the ones that present the strongest affinity toward OBP. Compound **3** is also the compound that presents the strongest affinity toward AChE than all the other eugenol derivatives studied.

When bound to OBP the ligands are mainly stabilized by Trp105, Leu67 and Ile78. When bound to AChE, the main interacting residues are Trp81, Tyr69 and Tyr322.

3. Material and Methods

3.1. Typical Procedure for the Preparation of Compounds 2a,b (Illustrated for 2b).

4-Allyl-2-methoxyphenol **1** (0.500 g, 3.05 × 10^{-3} mol, 1 equiv) was added dropwise to 2 M NaOH solution (3.37 mL) at room temperature. The mixture was kept under stirring until a homogeneous green solution was formed. To this mixture, 4-nitrobenzoyl chloride (0.622 g, 3.36 × 10^{-3} mol, 1.1 equiv) was added and the reaction was kept under stirring for 12 hr. After this period, the obtained solid was filtered and recrystallized (ethyl acetate/*n*-hexane), giving 4-allyl-2-methoxyphenyl 4-nitrobenzoate **2b** as a white solid (0.463 g, 49% yield). R_f = 0.62 (silica: dichloromethane), m.p. = 59–61 °C. ^{1}H NMR (CDCl$_3$, 400 MHz): δ_H 3.43 (2H, d, *J* = 6.4 Hz, CH$_2$Ph), 3.82 (3H, s, OCH$_3$), 5.12–5.20 (2H, m, CH=CH$_2$), 5.95–6.03 (1H, m, CH=CH$_2$), 6.83 (1H, d, *J* = 2.0 Hz, H-3), 6.86 (1H, dd, *J* = 4.4 and 2.0 Hz, H-5), 7.09 (1H, d, *J* = 8.0 Hz, H-6), 8.32–8.41 (4H, m, 4 × H Ph-NO$_2$) ppm. ^{13}C NMR (CDCl$_3$, 100 MHz): δ_C 40.11 (CH$_2$Ph), 55.48 (OCH$_3$), 112.86 (C-5), 116.31 (CH=CH$_2$), 120.79 (C-3), 122.32 (C-6), 123.62 (2 × H-Ph-NO$_2$), 131.40 (2 × H Ph-NO$_2$), 134.96 (C-1 Ph-NO$_2$), 136.91 (CH=CH$_2$), 137.73 (C-4), 139.64 (C-1), 150.77 (C-2), 150.81 (C-4 Ph-NO$_2$), 163.02 (C=O) ppm.

3.2. Synthesis of Compound 2c

A mixture of 4-allyl-2-methoxyphenol **1** (0.500 g, 3.05×10^{-3} mol, 1 equiv), DMAP (0.075 g, 6.1×10^{-4} mol. 0.2 equiv), and DCC (0.944 g, 4.56×10^{-3} mol, 1.5 equiv) was added to *p*-anisic acid (0.703 g, 4.58×10^{-3} mol, 1.5 equiv) in dichloromethane (5 mL). The reaction mixture was stirred at room temperature for 24 hr. At the end of this period, the white suspension obtained was filtered and the liquid phases were washed successively with 5% (*w/v*) hydrochloric acid (2 × 5 mL), 5% sodium hydrogen carbonate (*w/v*; 3 × 5 mL), and water (3 × 5 mL). Finally, after drying with anhydrous sodium sulfate, the organic phases were evaporated under reduced pressure to give 4-allyl-2-methoxyphenyl 4-methoxybenzoate **2c** as white solid (0.627 g, 69%). R_f = 0.49 (silica: dichloromethane), m.p. = 95–97 °C. ^{1}H NMR (CDCl$_3$, 400 MHz): δ_H 3.41 (2H, d, J = 6.8 Hz, CH$_2$Ph), 3.81 (3H, s, OCH$_3$), 3.90 (3H, s, Ph-OCH$_3$), 5.10–5.16 (2H, m, CH=CH$_2$), 5.95–6.03 (1H, m, CH=CH$_2$), 6.81 (1H, d, J = 2.0 Hz, H-3), 6.83 (1H, dd, J = 4.4 and 2.0 Hz, H-5), 6.99 (2H, d, J = 8.0 Hz, H-3 and H-5 Ph-OCH$_3$), 7.06 (1H, d, J = 8.0 Hz, H-6), 8.18 (2H, d, J = 9.2 Hz, H-2 and H-6 Ph-OCH$_3$) ppm. ^{13}C NMR (CDCl$_3$, 100 MHz): δ_C 40.11 (CH$_2$Ph), 55.48 (OCH$_3$), 55.89 (Ph-OCH$_3$), 112.85 (C-5), 113.74 (C-3 and C-5 Ph-OCH$_3$), 116.08 (CH=CH$_2$), 120.71 (C-3), 121.86 (C-1 Ph-OCH$_3$), 122.74 (C-6), 132.39 (C-2 and C-6 Ph-OCH$_3$), 137.15 (CH=CH$_2$), 138.31 (C-1), 138.86 (C-4), 151.19 (C-2), 163.75 (C-4 Ph-OCH$_3$), 164.62 (C=O) ppm.

3.3. Synthesis of Compound 3

4-Allyl-2-methoxyphenyl 4-nitrobenzoate **2b** (0.300 g, 9.58×10^{-4} mol, 1 equiv) was dissolved in dichloromethane (5 mL) at room temperature. The resulting solution was added dropwise to a solution of *m*-chloroperbenzoic acid (0.236 g, 1.37×10^{-3} mol, 1 equiv) in dichloromethane (5 mL) at 0°C (ice bath). After stirring for 1 hr, *m*-chloroperbenzoic acid was again added (0.236 g, 1.37×10^{-3} mol, 1 equiv), and the reaction mixture was stirred for more 12 h. A 10% aqueous solution of sodium sulfate (2 × 15 mL) was added, and the resulting mixture was washed with 5% aqueous solution of sodium hydrogen carbonate (2 × 15 mL). The organic phase was dried with anhydrous magnesium sulfate, the solvent was evaporated to give 2-methoxy-4-(oxiran-2-ylmethyl)phenyl 4-nitrobenzoate **3** as green solid (0.098 g, 31%). R$_f$ = 0.71 (silica: dichloromethane), m.p. = 59–61 °C. ^{1}H NMR (CDCl$_3$, 400 MHz): δ_H 2.59 (1H, q, J = 2.8 Hz, CH$_2$ oxirane), 2.74–2.92 (3H, m, CH$_2$Ph and CH$_2$ oxirane), 3.18–3.23 (1H, m, CH oxirane), 3.84 (s, 3H, OCH$_3$), 6.91 (1H, dd, J = 8 and 2 Hz, H-5), 6.95 (1H, d, J = 2.0 Hz, H-3), 7.12 (1H, d, J = 8 Hz, H-6), 8.35–8.41 (4H, m, 4 × H Ph-NO$_2$) ppm. ^{13}C NMR (CDCl$_3$, 100 MHz): δ_C 38.68 (CH$_2$Ph), 46.79 (CH$_2$ oxirane), 52.28 (CH oxirane), 55.91 (OCH$_3$), 113.33 (C-3), 121.20 (C-5), 122.49 (C-6), 123.64 (2 × C Ph-NO$_2$), 131.41 (2 × C Ph-NO$_2$), 134.88 (C-1 Ph-NO$_2$), 136.88 (C-4), 138.24 (C-1), 150.84 (C-2), 150.87 (C-4 Ph-NO$_2$), 162.96 (C=O) ppm.

3.4. Evaluation of Viability in Sf9 Cells

As a model, the *Spodoptera frugiperda Sf9* cell line was used. Cells were purchased from Sigma-Aldrich (St. Louis, MO, USA) and maintained in Grace's insect medium enriched with 10% fetal bovine serum (FBS) and 1% penicillin/streptomycin (Pen-Strep) at 28 °C. Cells were routinely subcultured as a suspension culture and assays conducted in the exponential growth phase.

For the assessment of viability, *Sf9* cells were plated at a density of 3.0×10^4 cells/well, followed by incubation for 24 h with the various compounds. After this period, a commercial solution of resazurin was added (Thermo Fisher A13261, final concentration: 1:10) and fluorescence was measured 60 min thereafter.

3.5. Inverted Virtual Screening Protocol Optimization

Considering the relevance of the target and year of publication, a search on Scopus was performed using the keywords: Virtual Screening (VS) and insecticide target. Seventeen studies were selected, and thirteen targets chosen for the inverted VS assays. The targets identified are listed in Table 1.

Table 1. List of targets selected for the inverted virtual screening study.

Target	Organism	PDB target	Resolution (Å)	Ref.
Acetylcholinesterase	*Aedes aegypti*	1QON	2.72	[8]
		4EY6	2.40	
	Drosophila melanogaster	1DX4	2.70	[9]
alpha-Esterase-7 (αE7)	*Lucilia cuprina*	5TYJ	1.75	[10]
		5TYP	1.88	
beta-*N*-Acetyl-D-hexosaminidase OfHex1	*Ostrinia furnacalis*	3NSN	2.10	[11]
		3OZP	2.00	[12]
Chitinase	*Ostrinia furnacalis*	3WL1	1.77	[13]
		3WQV	2.04	
Ecdysone receptor	*Heliothis virescens*	1R20	3	[14]
		1R1K	2.9	[15]
***N*-Acetylglucosamine-1-phosphate uridyltransferase (GlmU)**	*Xanthomonas oryzae*	2V0K	2.3	[16]
		2VD4	1.9	
Octopamine receptor	*Blattella germanica*	4N7C	1.75	[17]
Odorant Binding Protein	*Aedes aegypti*	5V13	1.84	[8]
	Drosophila melanogaster	2GTE	1.4	[18]
	Anopheles gambiae	3N7H	1.6	[19]
	Aedes aegypti	3K1E	1.85	
Peptide deformylase	*Xanthomonas oryzae*	5CY8	2.38	[20]
***p*-Hydroxyphenylpyruvate dioxygenase**	*Arabidopsis thaliana*	6ISD	2.4	[21]
Polyphenol oxidase	*Manduca sexta*	3HSS	2.7	[22]
Sterol carrier protein-2 (HaSCP-2)	*Helicoverpa armigera*	4UEI	Solution NMR	[23]
Voltage-gated sodium channel	*Periplaneta americana*	6A95	2.6	[24]

Each structure was extracted from the PDB database [25] and was prepared for docking using the Autodock Vina plugin for Pymol [26] with the removal of crystallographic waters and the extraction of ligands to separate files. The saved ligands were later used for active site coordinates and as reference for root mean square deviation (RMSD) calculations. In the absence of crystallographic ligands, the active site coordinates were obtained by selecting the most important active site residues. Re-docking was used as a quality measure, to evaluate the ability of the docking software in reproducing the geometry and orientation of the crystallographic pose.

The docking programs/scoring functions (SF) used were AutoDock Vina [27] and GOLD [28] (PLP, ASP, ChemScore, GoldScore). The protocol was optimized for each protein target and each SF, to minimize the RMSD values.

The optimized parameters for each SF consisted of the coordinates for the docking region centre, docking box dimension or radius, exhaustiveness, search efficiency, and number of runs. Once the RMSD values between poses (crystallographic and docked) were satisfactory (bellow 2 Å), the optimized conditions were used for the subsequent stages. The molecules were prepared for docking using Datawarrior [29] and OpenBabel [30] and were docked into each structure with all the five SF in study. A ranked list was prepared based on the average scores of each target.

Chem. Proc. **2021**, *3*, x FOR PEER REVIEW

8 of 11

3.6. Molecular Dynamics Simulations and Free Energy Calculations

Molecular dynamics simulations were performed on the four eugenol derivatives in complex with the two most promising targets identified from the inverted VS study: Odorant Binding Protein 1 (OBP—3K1E) and Acetylcholinesterase (AChE—1QON). The Amber18 software [31] was used throughout.

The complexes were treated with the Leap module of AMBER [32]. The protein targets were treated with the ff14SB force field [33], while the eugenol derivatives were parameterized using ANTECHAMBER, with RESP HF/6-31G(d) charges calculated with Gaussian [23,34] and the General Amber Force Field (GAFF) [35]. The complexes were placed in TIP3P water boxes with a minimum distance of 12 Å between the protein-surface and the side of the box and periodic boundary conditions were applied. Counter-ions (Na$^+$) were added to neutralize the overall charge and the complete systems.

To remove clashes prior to the MD simulation, four consecutive minimizations stages were performed with maximum of 2500 steps. Subsequently, the minimized systems were then subject to an equilibration procedure, divided into two stages: in the first stage (50 ps), the systems were gradually heated to 298 K using a Langevin thermostat at constant volume (NVT ensemble); in the second stage (50 ps) the density of the systems was further equilibrated at 298 K. Lastly, the production runs were performed for 100 ns, in a NPT ensemble at constant temperature (298 K, Langevin thermostat) and pressure (1 bar, Berendsen barostat). A 10 Å cutoff for nonbonded interactions was used along with the SHAKE algorithm, to constrain all covalent bonds. An integration time of 2.0 fs was applied. The final trajectories were analyzed using the cpptraj tool [36] and VMD [37], to confirm that all the systems were well equilibrated. The last 70 ns of the simulation were considered for hydrogen bonding analysis, and cluster analysis of the conformations generated.

In order to estimate the binding free energies of the protein-eugenol derivatives complexes, the molecular Mechanics / Generalized Born Surface Area method [38] was applied using the MM/PBSA.py [39] script from amber. The salt concentration applied was 0.100 mol dm^{-3}. From each MD trajectory, a total of 1400 conformations were taken from the last 70 ns and the contribution of the amino acid residues was estimated using the energy decomposition method.

4. Conclusions

In this work, three esters derived from eugenol and the corresponding oxirane from one of these esters were efficiently prepared. The obtained eugenol derivatives were subjected to biological activity evaluation in *Sf9* cell line, in order to predict their potential as natural based insecticides. We identified that the three derivatives esterified with a nitrobenzene were those showing higher potency, in some cases higher than the benchmark used.

In the present study, we report the application of an integrated molecular modelling—inverted virtual screening protocol for a selection of four eugenol derivatives in order to find possible protein targets in which they present insecticidal activity. After the target selection and protocol optimization, the eugenol derivatives were docked into each of the thirteen targets with five different SFs (PLP, ASP, ChemScore, GoldScore, Vina). Eugenol derivates showed an increased binding affinity for odorant binding proteins and acetylcholinesterases. The fact that there is, already, in the PDB database a structure of an OBP bound to eugenol, is a strong suggestion that eugenol derivates, could be used as repellents.

References

1. Lengai, G.M.W.; Muthomi, J.W.; Mbega, E.R. Phytochemical activity and role of botanical pesticides in pest management for sustainable agricultural crop production. *Sci. Afr.* **2020**, *7*, e00239.
2. Oliveira, J.L.; Campos, E.V.R.; Fraceto, L.F. Recent developments and challenges for nanoscale formulation of botanical pesticides for use in sustainable agriculture. *J. Agric. Food Chem.* **2018**, *66*, 8898–8913.
3. Salman, M.; Abbas, R.Z.; Israr, M.; Abbas, A.; Mehmood, K.; Khan, M.K.; Sindhu, Z.D.; Hussaind, R.; Saleemie, M.K.; Shaha, S. Repellent and acaricidal activity of essential oils and their components against *Rhipicephalus* ticks in cattle. *Vet. Parasitol.* **2020**, *283*, 109178.
4. Lee, M. Y. Essential oils as repellents against arthropods. *Biomed. Res. Int.* **2018**, *2018*, 6860271.
5. Fernandes, M.J.G.; Pereira, R.B.; Pereira, D.M.; Fortes, A.G.; Castanheira, E.M.S.; Gonçalves, M.S.T. New eugenol derivatives with enhanced insecticidal activity. *Int. J. Mol. Sci.* **2020**, *21*, 9257.
6. Ju, J.; Xie, Y.; Yu, H.; Guo, Y.; Cheng, Y.; Qian, H.; Yao, W. Analysis of the synergistic antifungal mechanism of eugenol and citral. *LWT Food Sci. Technol.* **2020**, *123*, 109128.
7. Spinelli, S.; Lagarde, A.; Iovinella, I.; Legrand, P.; Tegoni, M.; Pelosi, P.; Cambillau, C. Crystal structure of Apis mellifera OBP14, a C-minus odorant-binding protein, and its complexes with odorant molecules. *Insect Biochem. Mol. Biol.* **2012**, *42*, 41–50.
8. Ramos, R.S.; Costa, J.S.; Silva, R.C.; Costa, G.V.; Rodrigues, A.B.L.; Rabelo, E.M.; Souto, R.N.P.; Taft, C.A.; Silva, C.H.T.P.; Rosa, J.M.C.; et al. Identification of potential inhibitors from Pyriproxyfen with insecticidal activity by virtual screening. *Pharmaceuticals* **2019**, *12*, 20.
9. Riva, C.; Suzanne, P.; Charpentier, G.; Dulin, F.; Halm-Lemeille, M.-P.; Santos, J.S.-O. In silico chemical library screening and experimental validation of novel compounds with potential varroacide activities. *Pestic. Biochem. Physiol.* **2019**, *160*, 11–19.
10. Correy, G.J.; Zaidman, D.; Harmelin, A.; Carvalho, S.; Mabbitta, P.D.; Calaora, V.; Peter, J.; James, P.J.; Kotzeg, A.C.; Jackson, C.J.; et al. Overcoming insecticide resistance through computational inhibitor design. *Proc. Natl. Acad. Sci. USA* **2019**, *116*, 42, 21012–21021.
11. Liu, J.; Liu, M.; Yao, Y.; Wang, J.; Li, Y.; Li, G.; Wang, Y. Identification of novel potential β-*N*-Acetyl-D-Hexosaminidase inhibitors by virtual screening, molecular dynamics simulation and MM-PBSA calculations. *Int. J. Mol. Sci.* **2012**, *13*, 4545–4563.
12. Dong, L.; Shen, S.; Xu, Y.; Wang, L.; Yang, Q.; Zhang, J.; Lu, H. Identification of novel insect β-*N*-acetylhexosaminidase OfHex1 inhibitors based on virtual screening, biological evaluation, and molecular dynamics simulation. *J. Biomol. Struct. Dyn.* **2021**, *39*, 1735–1743.
13. Dong, Y.; Jiang, X.; Liu, T.; Ling, Y.; Yang, Q.; Zhang, L.; He, X. Structure-based virtual screening, compound synthesis, and bioassay for the design of chitinase inhibitors. *J. Agric. Food Chem.* **2018**, *66*, 3351–3357.
14. Hu, X.; Yin, B.; Cappelle, K.; Swevers, L.; Smagghe, G.; Yang, X.; Zhang, L. Identification of novel agonists and antagonists of the ecdysone receptor by virtual screening. *J. Mol. Graph Model.* **2018**, *81*, 77–85.
15. Harada, T.; Nakagawa, Y.; Ogura, T.; Yamada, Y.; Ohe, T.; Miyagawa, H. Virtual screening for ligands of the insect molting hormone receptor. *J. Chem. Inf. Model.* **2011**, *51*, 296–305.
16. Min, J.; Lin, D.; Zhang, Q.; Zhang, J.; Yu, Z. Structure-based virtual screening of novel inhibitors of the uridyltransferase activity of Xanthomonas *oryzae* pv. *oryzae* GlmU. *Eur. J. Med. Chem.* **2012**, *53*, 150–158.
17. Offermann, L.R.; Chan, S.L.; Osinski, T.; Tan, Y.W.; Chew, F.T.; Sivaraman, J.; Mok, Y.-K.; Minor, W.; Chruszcz, M. The major cockroach allergen Bla g 4 binds tyramine and octopamine. *Mol. Immunol.* **2014**, *60*, 86–94.
18. Laughlin, J.D.; Ha, T.S.; Jones, D.N.M.; Smith, D.P. Activation of pheromone-sensitive neurons is mediated by conformational activation of pheromone-binding protein. *Cell* **2008**, *133*, 1255–1265.
19. Oliferenko, P.V.; Oliferenko, A.A.; Poda, G.I.; Osolodkin, D.I.; Pillai, G.G.; Bernier, U.R.; Tsikolia, M.; Agramonte, N.M.; Clark, G.G.; Linthicum, K.J.; et al. Promising *aedes aegypti* repellent chemotypes identified through integrated QSAR, virtual ccreening, synthesis, and bioassay. Oliveira PL, ed. *PLoS ONE* **2013**, *8*, e64547.
20. Joshi, T.; Joshi, T.; Sharma, P.; Chandra, S.; Pande, V. Molecular docking and molecular dynamics simulation approach to screen natural compounds for inhibition of *Xanthomonas oryzae pv. Oryzae* by targeting peptide deformylase. *J. Biomol. Struct. Dyn.* **2021**, *39*, 823–840.
21. Fu, Y.; Liu, Y.-X.; Kang, T.; Sun, Y.-N.; Li, J.-Z.; Ye, F. Identification of novel inhibitors of *p*-hydroxyphenylpyruvate dioxygenase using receptor-based virtual screening. *J. Taiwan Inst. Chem. Eng.* **2019**, *103*, 33–43.

22. Fattouch, S.; Raboudi-Fattouch, F.; Ponce, J.V.G.; Forment, J.V.; Lukovic, D.; Marzouki, N.; Vidal, D. R. Concentration dependent effects of commonly used pesticides on activation versus inhibition of the quince (*Cydonia Oblonga*) polyphenol oxidase. *Food Chem. Toxicol.* **2010**, *48*, 957–963.

23. Cai, J.; Du, X.; Wang, C.; Lin, J.; Du, X. Identification of Potential Helicoverpa armigera (*Lepidoptera: Noctuidae*) Sterol Carrier Protein-2 Inhibitors through High-Throughput Virtual Screening. *J. Econ. Entomol.* **2017**, *110*, 1779–1784.

24. Shen, H.; Li, Z.; Jiang, Y.; Pan, X.; Wu, J.; Cristofori-Armstrong, B.; Smith, J.J.; Chin, Y.K.Y.; Lei, J.; Zhou, Q.; et al. Structural basis for the modulation of voltage-gated sodium channels by animal toxins. *Science* **2018**, *362*, 1–8.

25. Berman, H.M.; Westbrook, J.; Feng, Z.; Gilliland, G.; Bhat, T.N.; Weissig, H.; Shindyalov, I.N.; Bourne, P.E. The protein data bank. *Nucleic Acids Res.* **2000**, *28*, 235–242.

26. Seeliger, D.; de Groot, B.L. Ligand docking and binding site analysis with PyMOL and Autodock/Vina. *J. Comput. Aided Mol. Des.* **2010**, *24*, 417–422.

27. Trott, O.; Olson, A.J. AutoDock Vina: improving the speed and accuracy of docking with a new scoring function, efficient optimization, and multithreading. *J. Comput. Chem.* **2009**, *31*, 455–461.

28. Jones, G.; Willett, P.; Glen, R.C.; Leach, A.R.; Taylor, R. Development and validation of a genetic algorithm for flexible docking Edited by F. E. Cohen. *J. Mol. Biol.* **1997**, *267*, 727–748.

29. Sander, T.; Freyss, J.; von Korff, M.; Rufener, C. DataWarrior: an open-source program for chemistry aware data visualization and analysis. *J. Chem. Inf. Model.* **2015**, *55*, 460–473.

30. O'Boyle, N.M.; Banck, M.; James. C.A.; Morley, C.; Vandermeersch, T.; Hutchison, G.R. Open babel: an open chemical toolbox. *J. Cheminform.* **2011**, *3*, 33.

31. Case, D.A.; Cheatham, T.E., III; Darden, T.; Gohlke, H.; Luo, R.; Merz, K.M., Jr.; Onufriev, A.; Simmerling, C.; Wang, B.; Woods, R.J. The Amber biomolecular simulation programs. *J. Comput. Chem.* **2005**, *26*, 1668–1688.

32. Wang, J.; Wolf, R.M.; Caldwell, J.W.; Kollman, P.A.; Case, D.A. Development and testing of a general amber force field. *J. Comp. Chem.* **2004**, *25*, 1157–1174.

33. Maier, J.A.; Martinez, C.; Kasavajhala, K.; Wickstrom, L.; Hauser, K.E.; Simmerling, C. ff14SB: improving the accuracy of protein side chain and backbone parameters from ff99SB. *J. Chem. Theory Comput.* **2015**, *11*, 3696–3713.

34. Frisch, M.J.; Trucks, G.; Schlegel, H.B.; et al. Gaussian 09, Revision A.02. Published online 2016.

35. Wang, J.; Wang, W.; Kollman, P.A.; Case, D.A. Automatic atom type and bond type perception in molecular mechanical calculations. *J. Mol. Graph Model.* **2006**, *25*, 247–260.

36. Roe, D.R.; Cheatham, T.E. PTRAJ and CPPTRAJ: Software for processing and analysis of molecular dynamics trajectory data. *J. Chem. Theory Comput.* **2013**, *9*, 3084–3095.

37. Humphrey, W.; Dalke, A.; Schulten, K. VMD: Visual molecular dynamics. *J. Mol. Graph* **1996**, *14*, 33–38.

38. Wang, E.; Sun, H.; Wang, J.; Wang, Z.; Liu, H.; Zhang, J.Z.H.; Hou, T. End-point binding free energy calculation with MM/PBSA and MM/GBSA: strategies and applications in drug design. *Chem. Rev.* **2019**, *119*, 9478–9508.

39. Miller, B.R.; McGee, T.D.; Swails, J.M.; Homeyer, N.; Gohlke, H.; Roitberg, A.E. MMPBSA.py: an efficient program for end-state free energy calculations. *J. Chem. Theory Comput.* **2012**, *8*, 3314–3321.